by M. Datta

Anodic dissolution of metals at high rates

Electrochemical metal shaping and finishing processes involve anodic dissolution of metals at high rates. This paper presents a review of some fundamental aspects related to the understanding of such processes. Included are discussions of the phenomena of passive film breakdown that lead to the transpassive dissolution of metals, some of the available information on anodic reaction stoichiometry, and the role of convective mass transport and salt precipitation layers on metal removal rate and surface finish. The use of pulsating current permits the altering of anodic mass transport rates and transpassive dissolution behavior, thereby making it possible to obtain high dissolution efficiencies even at low average current densities.

Introduction

Several nonconventional machining processes such as electrochemical machining and electropolishing are based on the principle of electrochemical metal removal [1, 2]. These processes involve metal dissolution at high rates from a work piece which constitutes the anode in an electrolytic cell.

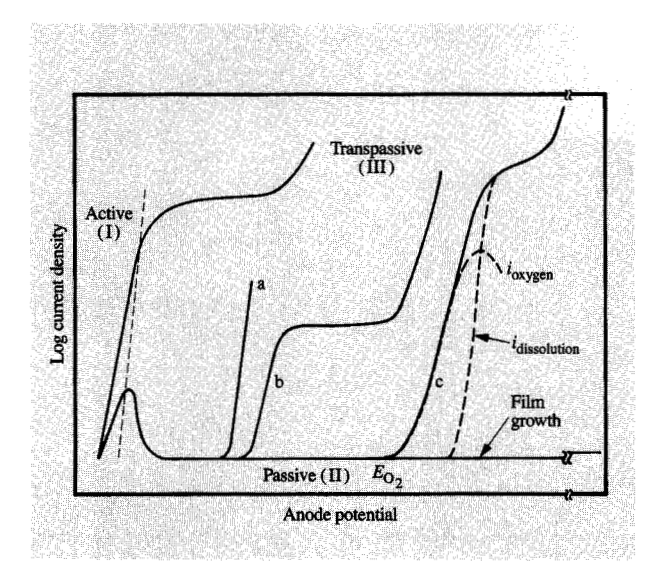
The highest known rate for an electrochemical process is achieved in electrochemical machining (ECM), with which

metal dissolution rates up to 10 mm/min are commonly attained. ECM is characterized by a high current density (10–300 A/cm²), a high electrolyte flow velocity (5–50 m/s), and a narrow interelectrode spacing (0.1–1 mm). A high electrolyte flow velocity is required to remove reaction products and to dissipate the heat generated. A close spacing is essential to reproduce the contours of the cathode onto the anode work piece. Neutral salt solutions are generally used as electrolytes.

Electropolishing also involves anodic metal dissolution, but the material removal rate is several orders of magnitude less than in ECM. It is generally employed as a finishing operation to remove surface roughness from a work piece, and therefore requires the removal of only small amounts of material. Electropolishing is usually carried out in concentrated acids with little or no electrolyte agitation, at current densities between 0.01 and 0.5 A/cm². The interelectrode spacing is not critical in electropolishing.

ECM and electropolishing have been successfully employed in aerospace, automobile, and other heavy industries for shaping, milling, deburring, and finishing. These processes are now receiving much attention in the electronics and other high-tech industries for the fabrication of microcomponents. Maskless and throughmask electrochemical micromachining (EMM) techniques are applicable to the processing of thin films and foils of materials that are difficult to machine by other methods [3–5].

Copyright 1993 by International Business Machines Corporation. Copying in printed form for private use is permitted without payment of royalty provided that (1) each reproduction is done without alteration and (2) the Journal reference and IBM copyright notice are included on the first page. The title and abstract, but no other portions, of this paper may be copied or distributed royalty free without further permission by computer-based and other information-service systems. Permission to republish any other portion of this paper must be obtained from the Editor.



Schematic representation of different types of anodic polarization behavior, showing active (I), passive (II), and transpassive (III) regions. Curve IIIa: localized breakdown by pitting; curve IIIb: electropolishing in concentrated acids; curve IIIc: transpassive oxygen evolution followed by metal dissolution at high rates in ECM electrolytes. E_{O_2} is the potential for oxygen evolution.

Depending on the metal-electrolyte combination and operating conditions, different anodic reactions take place at high current densities. Rates of these reactions are dependent to a great extent on the ability of the system to remove the reaction products as soon as they are formed and supply fresh electrolyte to the anode surface. All of these factors influence the machining performance—namely, the dissolution rate, shape control, and surface finish of the work piece. An understanding of the kinetics and stoichiometry of anodic reactions and their dependence on mass transport conditions is, therefore, essential in order to optimize relevant ECM and electropolishing parameters. In the following, the available literature on the anodic dissolution behavior of some of the technically important metals and alloys is reviewed.

Anodic polarization behavior

When the potential of an anode is increased, several different anodic reactions may take place [6-8], as shown schematically in **Figure 1**. At low potentials, where the current density increases with increasing anode potential, active dissolution of metal takes place (region I). In the passive potential region (II), a protective oxide film forms on the metal, indicated by a decrease in the current density until a very low current is observed. Several different types of anodic reactions may occur in the

transpassive potential region. In Figure 1, the transpassive region (III), beyond the passive region, is characterized by a renewed increase in the current density, independent of anodic reactions and their mechanisms. Localized passive film breakdown by pitting (IIIa) and electropolishing in concentrated acids (IIIb) involve transpassive metal dissolution at potentials less noble than that necessary for oxygen evolution. In concentrated neutral salt solutions that contain oxidizing anions such as nitrate or chlorate ions, oxygen evolution precedes transpassive metal dissolution. ECM in these solutions takes place at potentials much higher than that required for oxygen evolution (IIIc).

The polarization curves of Figure 1 qualitatively describe different possible anodic behaviors of metals and alloys in different electrolytes. In some cases, however, the actual shape of anodic polarization curves may be slightly different from those shown. For example, several metals and alloys may become passivated immediately after they are exposed in a passivating electrolyte. In such systems, the active region is generally absent in the polarization curve, exhibiting only the passive–transpassive transition.

In the ECM literature, neutral salt solutions are generally categorized into two types: passivating (electrolytes containing nitrates, chlorates) and nonpassivating (electrolytes containing chlorides, bromides). However, this distinction is mostly applicable only to iron and nickel [9, 10]. Other metals such as copper, titanium, and aluminum display qualitatively similar polarization behavior in both types of electrolytes.

A limiting current plateau is usually observed in each of the types of polarization curves of Figure 1. The importance of the limiting current and its influence on ECM and electropolishing performance are discussed later in greater detail. At potentials greater than the limiting current, several new anodic reactions can occur. Anodic polarization of certain metals in concentrated acids at a current beyond the limiting current may lead to simultaneous production of oxygen. In *nonpassivating* ECM electrolytes (e.g., in concentrated NaCl), a change in dissolution valence may occur.

From the above discussion, it is clear that the anodic behavior of metals at high potentials involves a variety of processes, the nature and rate of which may be influenced by electrochemical and hydrodynamic parameters. To acquire an understanding of these processes, experimental investigations must be performed in properly designed electrochemical cells that can provide controlled hydrodynamic conditions at the anode. Rotating disk electrodes have frequently been employed for the study of electropolishing [11, 12]. However, they are not suitable for high-rate dissolution studies under ECM conditions, particularly in systems in which metal dissolution is

preceded or accompanied by oxygen evolution. Flow channel cells have been used effectively for high-rate dissolution studies, under ECM conditions, of different metals and alloys in passivating as well as nonpassivating electrolytes [9, 10, 13, 14].

Active dissolution

The anodic current in region I of Figure 1 (the active region) is due to a dissolution reaction that corresponds to the direct passage of metal atoms into the electrolyte in hydrated or complexed form. The active dissolution involves the removal of atoms from energetically favored kink sites on monoatomic steps situated on closed packed planes [15, 16]. For these reasons, the rate of active dissolution at a given potential depends on the crystal planes involved. Since the atoms situated in the proximity of grain boundary and other crystalline defects are energetically more favorable, they are preferentially removed during active dissolution. Studies of the dissolution kinetics and morphology of low index planes of iron single crystal have demonstrated that a strong correlation exists between the kinetics of dissolution of an iron electrode and the atomistic structure of its surface. The dissolved surface morphology has been described quantitatively in terms of monoatomic steps and kinks [15, 16]. The surface concentration of kinks depends strongly on the electrode potential, while the step density is determined by the pH level of the solution. On randomly oriented crystals or in the presence of a high density of imperfections, the nucleation of monoatomic steps is rapid. Monoatomic steps moving at different velocities lead to the formation of microscopically observable etch patterns. Active dissolution thus leads to surface etching even under extremely high current densities.

In the potential region in which the metal dissolution rate is not limited by mass transport, the kinetics of active dissolution is generally expressed by Tafel behavior. Highrate electrodissolution kinetics of nickel and iron have been studied in chloride solutions [17-19]. Polarization measurements for nickel in neutral and acidified NaCl solutions have yielded a Tafel slope between 80 and 90 mV/decade, independent of pH level [17]. These values are in agreement with a dissolution mechanism involving the complex formation of the dissolved species with chloride and hydroxyl ions [20]. In slightly alkaline solutions, passivation effects lead to apparently higher Tafel slopes. The influence of chloride ions and pH levels on the anodic dissolution of iron has been investigated over a wide range of H⁺ and Cl⁻ concentrations [19]. Depending on the polarization conditions, pH level, and chloride ion concentration, the Tafel slope was found to vary between 0.04 mV and 0.11 mV, suggesting the formation of several chloro-iron complexes as adsorbed reaction intermediates [19].

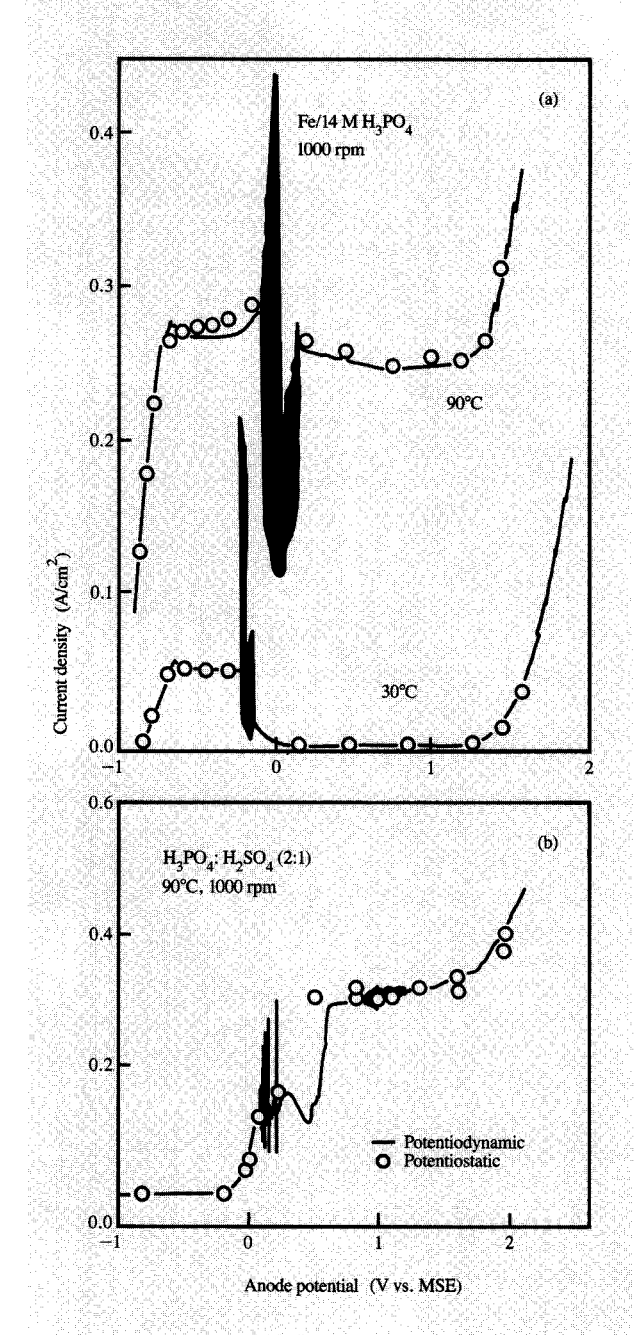
Passivation

In the passive region (Figure 1, region II), the anode surface is covered by an oxide film that protects the surface from high-rate dissolution. The dissolution current in the passive potential region is controlled by the rate of dissolution of the passive film, which in turn depends on the ionic conductivity of the film and its solubility in the electrolyte. In general, the passive current is of the order of μ A/cm² and is independent of applied potential in the passive potential range. The thickness, composition, and electrical properties of passive films depend on the metal involved, the solution, and the applied potential.

Properties of passivating films on different types of metals have been extensively studied because of their importance in corrosion control [21]. In the following, a brief review is presented of passivating films on nickel and iron in ECM and electropolishing electrolytes.

When immersed in aqueous solutions, nickel spontaneously passivates and becomes covered with a film of Ni(OH), [22, 23]. Upon anodic polarization, depending on the potential and the pH of the electrolyte, oxides such as NiO, Ni₂O₄, Ni₂O₃, and NiO, of different structures and degrees of hydration may form [24]. Evidence for the existence of divalent and trivalent nickel oxide has been produced by a number of authors [23, 25-27]. According to Dickinson et al. [27], the film present on nickel in the passive potential region is composed of NiO and Ni(OH), the former being the passivating species. In the potential range preceding oxygen evolution, Ni(OH), and β -Ni(OH), are usually present [25, 26]. Several authors have reported the oxidation state of nickel oxide to be NiO_{1.7-1.9} [23, 28], by assuming the oxide to be a solid solution of NiO, and Ni₂O₃. Passive film thicknesses on nickel are extremely thin; typical values as reviewed in [29] vary between 4 and 60 Å.

Anodic polarization of iron in sulfuric acid leads to the formation of passive films with an average film thickness of less than a monolayer at the passivation potential. The passive film thickness, however, increases with increasing potential with values up to several nanometers at potentials below the oxygen evolution region. The composition of anodic passive films on iron has been investigated by a number of workers using electrochemical, chemical, and surface analytical techniques [30-34]. Nagayama and Cohen [31, 32] proposed a sandwich model consisting of an inner layer of Fe₂O₄ and an outer layer of γ -Fe₂O₃. The existence of these oxides has been confirmed by electron diffraction [31–33]. According to Vetter [34], the potential drop in a passive film is across the outer layer, since Fe₂O₄ is a good electronic conductor. Bloom and Goldenberg have reported that y-Fe₂O₃ is stable only if it contains a minimum concentration of hydrogen ions [35]. Indeed, there are indications in the literature that the outer layer



Anodic polarization behavior of iron in concentrated phosphoric acid at two different temperatures (a) and in a mixture of phosphoric-sulfuric acids (b); measurements were performed using a rotating disk electrode rotating at 1000 rpm. The anode potential was measured against a mercury sulfate reference electrode (MSE). Note that the metal dissolution rate in phosphoric acid is extremely sensitive to temperature, and that the addition of sulfuric acid to phosphoric acid completely suppresses the active dissolution of iron. Parts (a) and (b) from [39] and [42], respectively; reproduced with permission from Pergamon Press.

contains hydrogen in the form of hydroxyl ions or water [35, 36].

Passive films formed on aluminum and titanium are generally relatively less conducting; hence, the application of high anodic potentials leads to film growth. Anodization of these metals in some electrolytes may yield films having a thickness of the order of several μ m that can withstand potentials greater than 100 V [21].

• Transpassivity

The stability of passive films and the reactions taking place in the transpassive potential region depend on the nature of the anode potential and the anions present. For example, in the presence of aggressive anions (such as chloride ions) many metals exhibit localized film breakdown and dissolution by pitting when their potential exceeds the critical pitting potential (IIIa). Pitting phenomena, which are of great technical importance in corrosion, have been studied extensively [37]. Under high field conditions in the film and at the film–solution interface, aggressive anions may penetrate through defects in the film and may provoke its localized destruction, leading to transpassive dissolution from the bare surface. Under these conditions the metal dissolves with the same oxidation state as that observed in the active mode.

In some cases, transpassive dissolution may involve film oxidation to soluble species. A well-known example is the transpassive dissolution of chromium in sulfuric acid [38]. In the passive potential region, the chromium surface is covered with a thin oxide film of trivalent chromium which protects the metal. In the transpassive potential region, the trivalent oxide film is transformed to an oxide of hexavalent chromium, which is highly soluble, namely

$$Cr_2O_3 + 4H_2O \rightarrow Cr_2O_7^{2-} + 8H^+ + 6e^-.$$
 (1)

Chromium, therefore, goes into solution as chromate during the transpassive dissolution of chromium. The transpassive dissolution of chromium in concentrated phosphoric-sulfuric acids also involves the formation of soluble chromate. On the other hand, the transpassive dissolution of iron in concentrated acids is initiated by a pitting mechanism [39]. Pitting-induced transpassive dissolution has been observed in many other electropolishing systems [6, 40, 41].

On passive films that are relatively stable and exhibit electronic conduction, oxygen evolution takes place by solution oxidation upon anodic polarization into the transpassive potential, namely

$$2H_2O \rightarrow O_2 + 4H^+ + 4e^-.$$
 (2)

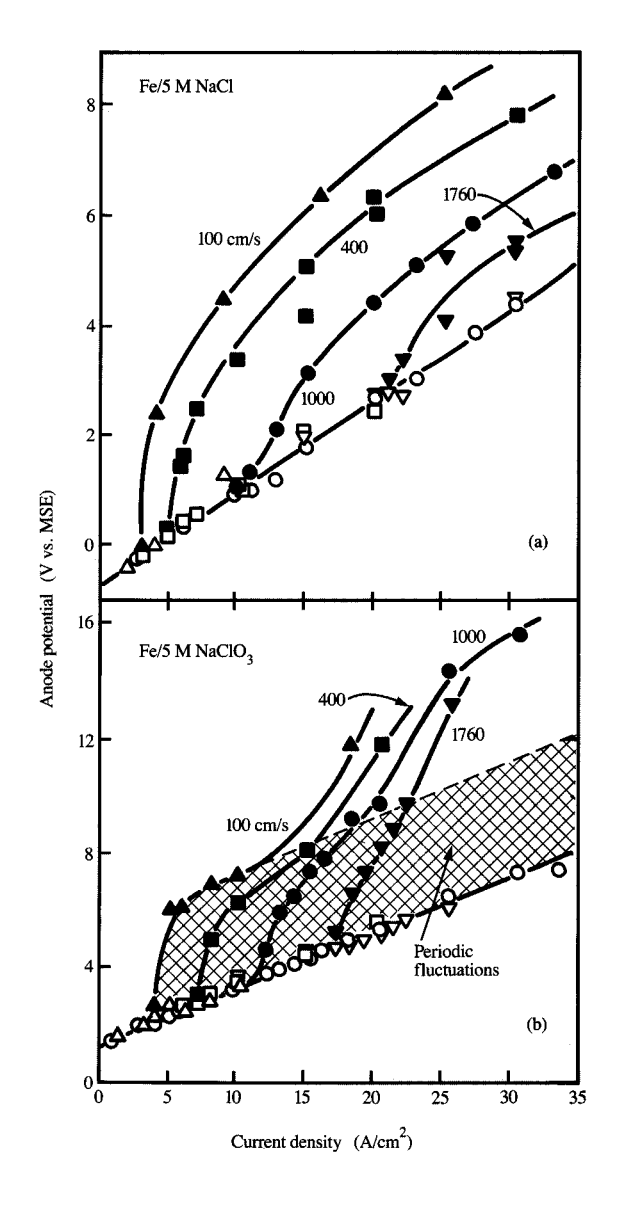
In these metal-electrolyte systems, transpassive metal dissolution sets in at potentials much higher than the potential for oxygen evolution. At still higher potentials, very high metal dissolution rates may be reached.

Typical anodic polarization curves obtained during electropolishing and ECM studies are shown in Figure 2 and Figure 3. Anodic polarization curves shown in Figure 2 were obtained with a rotating disk electrode [39, 42]. Figure 2(a) demonstrates the influence of temperature on the polarization behavior and the metal dissolution rate during electropolishing of iron in concentrated phosphoric acid [39]. At 90°C, the current density rises sharply in the active region until a limiting plateau is observed which is followed by a region of current fluctuations. At higher potentials, a second limiting current plateau is observed, and finally, at still higher potentials, a sharp increase in current occurs, accompanied by oxygen evolution. The magnitudes of both limiting currents increase with increasing rotation speed [39]. At 30°C, the polarization behavior at low anodic potentials is qualitatively similar to that at 90°C, except for the magnitude of the anodic current, which is relatively very low. Beyond the current fluctuation region, anodic passivation occurs, as indicated by a sharp drop in the current. At higher potentials oxygen evolution occurs. Metal dissolution at 30°C is insignificant over a wide range of potential. These polarization curves help to explain why electropolishing of iron and iron-based alloys in phosphoric acid is best achieved at elevated temperatures [2, 11, 12, 39, 42]. Figure 2(b) shows that the addition of sulfuric acid to the phosphoric acid completely suppresses the active dissolution of iron [42]. Metal dissolution in this solution occurs only in the transpassive potential region.

Figure 3 contains galvanostatic polarization data for iron in concentrated sodium chloride and sodium chlorate solutions. The data were obtained in a flow channel cell apparatus with a back-side capillary arrangement for potential measurements [9, 10]; the applied current density ranged up to 35 A/cm². At low current densities a linear current–potential relationship was observed, the measured potential being dominated mainly by the ohmic drop between the anode and the capillary. In both the systems, a limiting current was observed, the value of which was dependent on the electrolyte flow velocity. In the chlorate solution, the limiting current was followed by a region of periodic potential oscillations.

Anodic reaction stoichiometry

A complete analysis of all reaction products is required in order to obtain information on the anodic reactions taking place at high potentials. This, however, is not easily accomplished, since it may require the collection of solid, dissolved, and gaseous products in a flow system. Furthermore, separation of the anodic products from the cathodic reaction products is not easily possible. In ECM and electropolishing, a knowledge of anodic reactions taking place at high potentials is derived primarily from weight loss measurements and applying the Faraday law



Flaure 3

Galvanostatic anodic polarization curves for iron in 5 M NaCl (a) and 5 M NaClO₃ (b) in a flow channel cell, at different flow velocities [9, 10]. A flow-dependent limiting current was observed in both solutions.

[8–14, 39, 42]. The weight loss, ΔW , is related to the metal dissolution stoichiometry by

$$\Delta W = \frac{ItM}{nF},\tag{3}$$

where I is the applied current, t is the time, F is the Faraday constant, and n is the valence of metal dissolution

211

Table 1 Metal dissolution valence in electropolishing and ECM systems.

Metal	Electrolyte	Dissolution valence		Oxygen evolution	Reference
		Active	Transpassive		
Electropolish	ing systems				
Fe	H_3PO_4	2	3	yes	39
Fe	$H_3PO_4 + H_2SO_4$	_	2 and 3	yes	42
Cu	H ₃ PO ₄	2	2	yes	70
Cr	H ₃ PO ₄	_	6	no	59
Cr	$H_3PO_4 + H_3SO_4$	_	6	no	59
Ni	H,SO,	2	2	yes	8
Ti	HClO₄	_	1.8*	no	58
ECM systems	3				
Ni	NaCl	2	2	no	9, 17
Fe	NaCl	2	2 and 3	no	9, 43
Ni, Fe	NaNO ₂		2	yes	10, 47, 50
Ni, Fe	NaClO,	_	2 and <2*	yes	10, 43
Cr	NaCl, NaÑO,		6	no	54, 55
Cu	KCl	1	1 and 2	no	13, 14
Cu	KNO_3 , K_2SO_4	2	2 and 1	no	13, 14
Ti	NaCl, NaBr		4	no	58
Mo	KOH, K,CO,		6	no	56, 57

^{*}Anion reduction at the anode

(the number of electrons removed from dissolving metal atoms by anodic oxidation). The use of weight loss as a measure of dissolution valence is strictly applicable to anodic reactions involving metal dissolution only. In the presence of other reactions occurring simultaneously at the anode, such as oxygen evolution, weight loss measurements have frequently been used to determine an "apparent dissolution valence" [9-12, 42]. Under these conditions, a knowledge of current efficiency is required to calculate n using Equation (3).

The value of n provides information on the overall reaction stoichiometry. Its measurement is, therefore, a prerequisite for any mechanistic studies. From a practical point of view, a knowledge of the value of n is useful for the calculation of metal removal rate. Typical values of n for different metals under ECM and electropolishing conditions are given in **Table 1**.

During the high-rate dissolution of copper, the value of n undergoes a noticeable change with the transition from active to transpassive dissolution. The anodic polarization of copper does not exhibit the conventional passivation behavior, as described earlier. Transpassive dissolution here refers to dissolution at current densities higher than the limiting current for salt film formation. In nitrate and sulfate solutions, active dissolution proceeds with a dissolution valence of 2. Transpassive dissolution leads to simultaneous production of monovalent copper reaching a limiting value of 1.6 at high current densities [13, 14]. The active dissolution of copper in chloride solution proceeds with a dissolution valence of 1. This is due to the

stabilization of cuprous ions by complex formation. In the transpassive mode, simultaneous formation of cupric ions increases the apparent dissolution valence, going through a maximum of 1.4 before reaching a limiting value of 1.2 at high current densities. No oxygen evolution has been reported during copper dissolution in these electrolytes [14].

High-rate dissolution of iron in a chloride solution at low current densities involves iron dissolution in its divalent state [9, 43]. However, at current densities higher than the limiting current density (Figure 3), simultaneous production of Fe²⁺ and Fe³⁺ takes place [9, 43]. This has been confirmed by the complete analysis of reaction products which have shown no evidence of anodic oxygen evolution during high-rate dissolution of iron in concentrated chloride solutions [43]. High-rate anodic dissolution of nickel in chloride solutions involves the formation of divalent nickel ions independently of the current density level [9, 17].

Anodic reaction stoichiometry during the high-rate dissolution of iron and nickel in *passivating* ECM solutions (sodium nitrate and sodium chlorate) has been studied extensively [10, 43–50]. In these studies, oxygen evolution has been found to be the predominant anodic reaction at relatively low current densities in the transpassive potential region. At higher current densities, the relative rate of metal dissolution increases with increasing current density. This is shown in part (a) of **Figure 4**, which contains apparent dissolution valence data for iron dissolution in nitrate and chlorate electrolytes. For

comparison purposes, the dissolution valence in chloride solution is included. In ECM, the distribution of metal dissolution rate on the work piece determines its final shape in relation to the tool [51, 52]. The machining performance is, therefore, influenced significantly by the dependence on current density of the anodic reactions. For example, *passivating* metal-electrolyte systems are known to give better ECM precision because of their ability to form oxide films and evolve oxygen in the stray-current region [51-53].

It is interesting to note that during the high-rate dissolution of iron in the chlorate solution, the apparent dissolution valence was found to be less than 2 at high current densities. Similar results have been obtained for the high-rate dissolution of nickel in chlorate solution [10]. Such anomalous behavior may result from intergranular attack, leading to removal of metallic particles from the anode, or they may be the result of chemical reactions occurring at the anode surface. X-ray diffraction analysis of dissolution products has not shown any evidence of the presence of metallic particles [17]. The low dissolution valence values have been attributed to chlorate reduction at active sites on the anode by the corrosion reactions

$$2\text{Fe} + \text{ClO}_3^- + 6\text{H}^+ \rightarrow 2\text{Fe}^{3+} + \text{Cl}^- + 3\text{H}_2\text{O}$$
 (4)

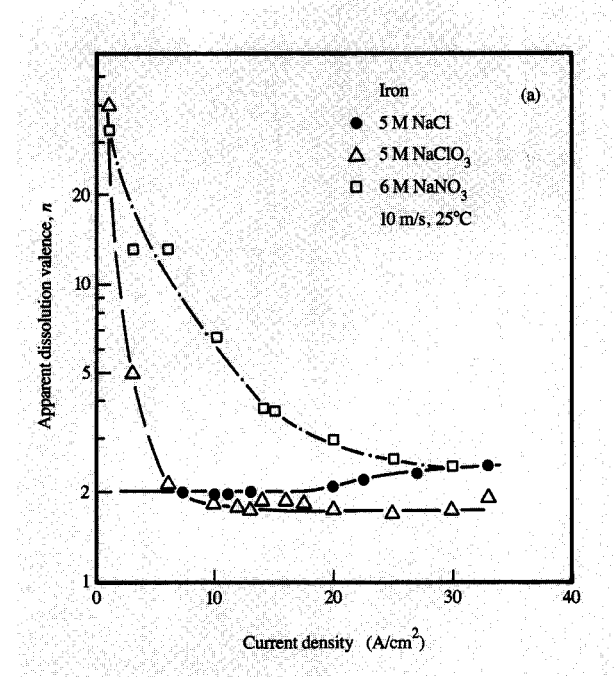
and

$$6Fe^{2+} + ClO_3^- + 6H^+ \rightarrow 6Fe^{3+} + Cl^- + 3H_2O.$$
 (5)

Solution analysis, indeed, has shown an accumulation of Cl⁻, providing conclusive evidence of chlorate reduction on the active surface produced during the high-rate anodic dissolution of iron and nickel, and thus also providing an explanation for the experimentally obtained anomalous dissolution valence [10].

Anodic dissolution of Cr in ECM electrolytes takes place in the transpassive potential region, yielding Cr⁶⁺; the dissolution valence is independent of current density and the nature of the electrolyte anion [54, 55]. Molybdenum also yields Mo⁶⁺ during anodic dissolution, which takes place exclusively in the transpassive potential region [56, 57]. The high-rate anodic dissolution of titanium takes place at sufficiently high anode potentials through the breakdown of passive films. In chloride and bromide solutions, the dissolution valence is close to 4, similar to that found under pitting corrosion conditions [58].

In concentrated sulfuric acid, the transpassive dissolution of nickel occurs at potentials well below that required for oxygen evolution; the associated metal dissolution valence is 2. At higher current densities, oxygen evolution occurs, and the sum of the current efficiencies for metal dissolution based on Ni²⁺ formation and oxygen evolution is 100% [8]. The transpassive dissolution of Cr in concentrated phosphoric acid and a mixture of concentrated phosphoric and sulfuric acids



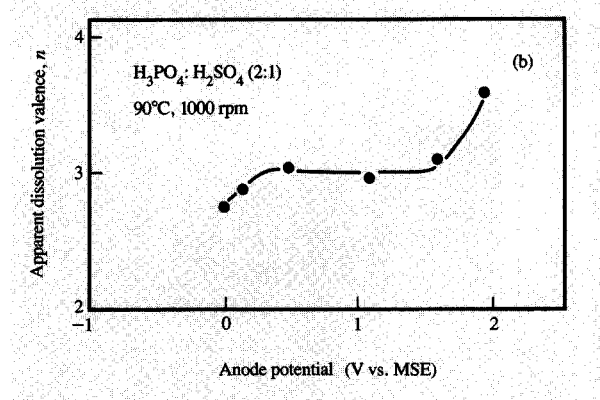


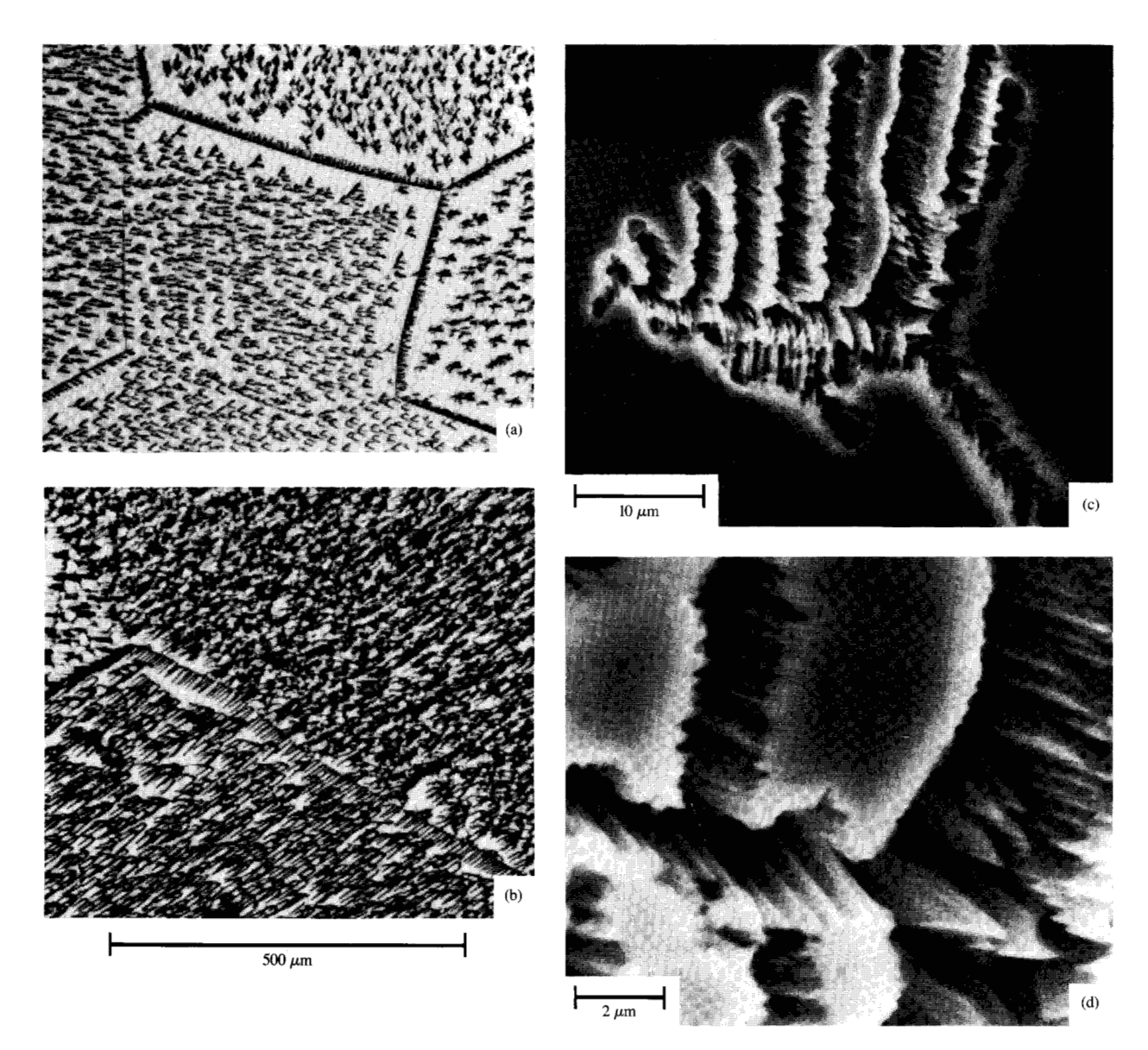
Figure 4

Apparent dissolution valence data for iron (a) in neutral salt solutions obtained in a flow channel cell at an electrolyte flow velocity of 10 m/s [9, 10], and (b) in a mixture of phosphoric-sulfuric acids using a rotating disk electrode rotating at 1000 rpm [42]. In 5 M NaCl, simultaneous production of Fe²⁺ and Fe³⁺ takes place at current densities higher than the limiting current. In nitrate and chlorate solutions, oxygen evolution is the dominant anodic reaction at low current densities; high-rate metal dissolution occurs at high current densities. In the phosphoric-sulfuric acids mixture, metal dissolution is followed by oxygen evolution.

yields a dissolution valence of 6, independently of anode potential [59].

Anodic reaction stoichiometry for iron dissolution in concentrated phosphoric acid depends on the anode potential [39]. In the active region and in the current plateau region below current fluctuations [Figure 2(a)], iron

213



Microphotographs showing the initiation of transpassive nickel dissolution in 5 M NaNO₃ + 1 M HNO₃. Dissolution experiments were performed in a flow channel cell at 5 A/cm², a flow velocity of 10 m/s, and two different dissolution times: (a) 0.49 s and (b) 1.01 s. Transpassive dissolution is initiated by localized breakdown of passive films at discrete sites. With increased dissolution time, the dissolution sites grow and merge, producing a rough surface. Microphotographs (c) and (d) show that transpassive dissolution takes place from a few well-defined crystallographic planes. From [50], reprinted by permission of the publisher, The Electrochemical Society, Inc.

dissolves as Fe^{2+} . In the potential region corresponding to current fluctuations, both Fe^{2+} and Fe^{3+} are formed, the measured value of n being 2.5. At potentials higher than that associated with the current fluctuations, iron dissolution leads to Fe^{3+} formation. At higher potentials, a renewed increase in current density is associated with oxygen evolution, as evidenced by apparent valence values of n in excess of 3 under these conditions. In a mixture of

concentrated phosphoric and sulfuric acids, the anodic dissolution of iron takes place exclusively in the transpassive potential region [Figures 2(b) and 4(b)]. At potentials below the current plateau [Figure 2(b)], the simultaneous production of Fe²⁺ and Fe³⁺ occurs, the latter becoming increasingly important until only Fe³⁺ is formed at the limiting current plateau. At potentials higher than the limiting current, apparent dissolution valence

values greater than 3 are due to simultaneous oxygen evolution [42].

During the high-rate dissolution of copper in concentrated phosphoric acids, copper dissolves as Cu^{2+} in the active region and in the current plateau region. At potentials higher than those of the current plateau region, simultaneous oxygen evolution occurs, yielding a value of n greater than 2. The transpassive dissolution of titanium in perchloric acid leads to an anomalous dissolution valence of 1.8; this has been explained by the reduction of perchlorate ions at the anode [58].

Transpassive film breakdown

From the above discussion it is clear that many ECM and electropolishing systems involve high-rate metal dissolution in the transpassive potential region, where the protective property of passive films is destroyed. Transpassive film breakdown leading to high-rate metal dissolution has been an interesting research topic. According to Mao [43], the oxide film formed on iron in chlorate solution dissolves under conditions of low pH at the anode, as a result of oxygen evolution. In a later work, Mao, LaBoda, and Hoare [60] explain the dissolution mechanism of iron in different passivating electrolytes in terms of an ion exchange model previously proposed by Hoar [6]. According to the model, electrolyte anions may be incorporated into the film lattice by exchanging positions with oxygen ions and thus facilitating film dissolution. No direct proof of the existence of such a mechanism exists thus far. A series of systematic studies of film breakdown phenomena have been conducted by Datta, Landolt, and Mathieu, leading to a better understanding of the transpassive metal dissolution mechanism [29, 50, 61-63]. The studies involved the use of extremely short dissolution time to investigate the initiation of transpassive dissolution, and the use of electrochemical and surfacesensitive analytical techniques to study the transpassive film thickness and composition over a wide range of current density, from conditions under which only oxygen evolution occurred to conditions leading to high-rate metal dissolution.

The application of a short anodic current pulse of varying intensity and duration showed that transpassive nickel dissolution is initiated at discrete breakdown sites, the number of which increases with applied current density [50]. Once initiated, the dissolution sites grow with time, as shown in **Figure 5**. Micropits reveal crystallographic planes from which dissolution takes place as under active dissolution conditions. The microphotographs of Figures 5(c) and 5(d) show that the nucleation sites grow in distinct directions by anodic dissolution from a few well-defined crystallographic planes. To further investigate the influence of crystallographic orientation on the dissolution process, experiments were performed using a single crystal with a

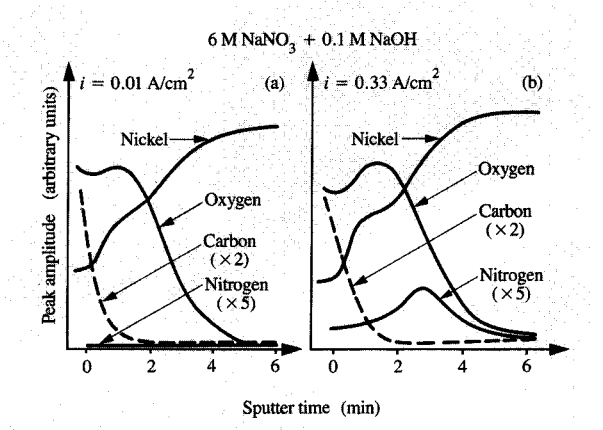


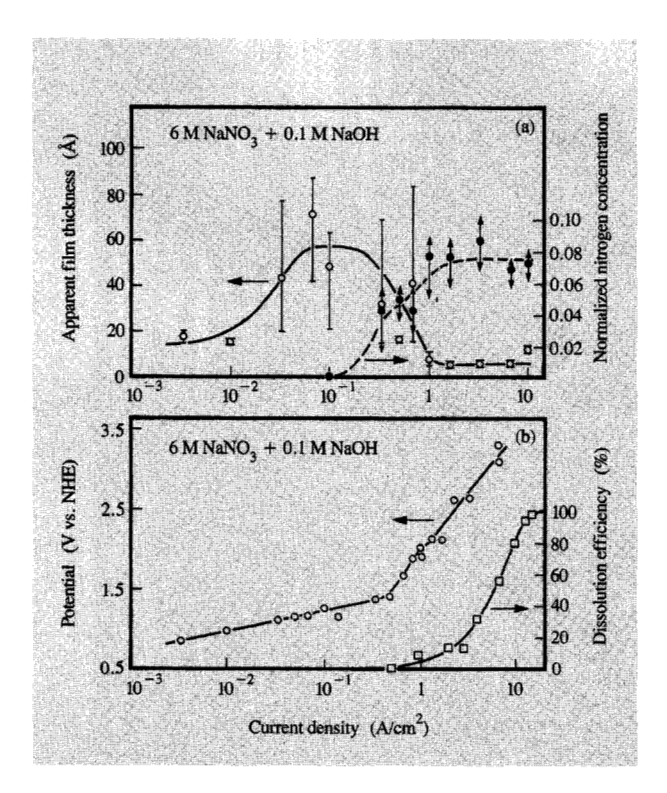
Figure 6

AES depth profiles of transpassive oxide films on a nickel single crystal with {111} orientation, formed in 6 M NaNO $_3$ + 0.1 M NaOH at two different current densities. A nitrogen maximum is observed at the metal–oxide interface at 0.33 A/cm², indicating that the transpassive films are permeable to nitrate ions under these conditions. From [29], reproduced with permission from Pergamon Press.

{111} orientation. Metal dissolution was found to proceed in three directions oriented approximately 120° to one another, corresponding to the {111} projections. This gave rise to Y-shaped dissolution sites [50]. These results conclusively demonstrated the important role of grain orientation during transpassive metal dissolution. Eventually the dissolution sites grow and merge, yielding a rough and etched surface.

Auger electron spectroscopy (AES), X-ray photoelectron spectroscopy (XPS), and coulometry have been employed to learn more about the thickness and composition of oxide films in the transpassive potential region [29, 61-63]. Figure 6 shows typical AES depth profiles obtained for nickel samples, polarized in a nitrate electrolyte at two current densities in the transpassive potential region. From the depth profile data, film thicknesses were determined at different current densities in the transpassive potential region. It is interesting to note that the transpassive film thickness undergoes a maximum in the oxygen evolution region and reaches a constant value at current densities at which transpassive dissolution takes place. Coulometry data have indicated a qualitatively similar behavior [29]. AES depth profiling has revealed a nitrogen maximum at the oxide-metal interface. The presence of nitrogen at the oxide-metal interface was also confirmed by angle-resolved XPS [61-63]. The nitrogen maximum at the interface [Figure 6(b)] was observed before transpassive dissolution set in.





Apparent thickness of transpassive films on single-crystal {111} nickel in 6 M NaNO₃ + 0.1 M NaOH and normalized nitrogen concentration at the interface as a function of current density (a). Anodic polarization and dissolution efficiency data are also included (b). Anode potential is indicated with respect to a normal hydrogen electrode (NHE). Note that the nitrogen concentration attains a limiting value and the transpassive films are very thin in the current density region in which metal dissolution occurs. From [29], reproduced with permission from Pergamon Press.

AES depth profile results as a function of current density are summarized in Figure 7. In Figure 7(a), the normalized value of nitrogen concentration is the ratio between the nitrogen peak amplitude and the nickel peak amplitude. The data of Figure 7 show that the relative amount of nitrogen in the film increases with increasing potential until a maximum value is reached, corresponding to conditions of high-rate dissolution. Similar results have been obtained for transpassive films on iron [63]. These findings are in contradiction with an ion-exchange mechanism which requires the maximum anion concentration to lie at the solution-film interface. The observed nitrogen concentration maximum at the film-metal interface is due to nitrate ion penetration through flaws in the film and local accumulation at the metal surface. The nitrogen in the film was found to be present in reduced form, most probably as N³⁺. This may have been due to the reaction of adsorbed nitrate with the

metallic surface during transpassive dissolution, as observed for nickel, iron, and titanium in chlorate and perchlorate solutions [10, 58].

Different studies related to transpassive films have indicated that transpassive metal dissolution efficiency is independent of film thickness [29, 63]. This can be explained by considering the fact that transpassive metal dissolution is initiated by a pitting mechanism. Such a mechanism involves two parallel paths for the anodic current: direct metal dissolution through pores and pits, and electron transfer through the oxide film, accompanied by oxygen evolution. High-rate transpassive metal dissolution at steady-state conditions, therefore, involves a delicate balance between depassivation and repassivation phenomena, which govern the extent to which the anode surface is covered by the oxide film and determine the current efficiency for metal dissolution [50].

Mass transport effects and salt film formation

During anodic dissolution, the concentration at the anode surface can be significantly different from that of the bulk. Since these concentrations are primarily determined by the rate of mass transport, transport mechanisms and diffusion layer thickness play an important role in high-rate anodic dissolution processes. Metal ions produced at the anode are transported into the solution by convective diffusion and migration. To maintain electroneutrality, electrolyte anions accumulate near the anode, causing the rate of convective diffusion away from the anode to be compensated by the rate of migration toward the anode. The extent of ion buildup depends on the current density, metal dissolution efficiency, and hydrodynamic conditions. As shown above, polarization at high potentials leads to a limiting current plateau in many ECM and electropolishing systems [9-14, 47, 49]. The limiting current density has been found to increase with increasing electrolyte flow in a channel cell or with increasing rotation speed in an RDE system. The limiting current density is, therefore, controlled by convective mass transport.

For an anodic reaction that is controlled by convective mass transport, the anodic current density, i, is given by

$$i = nFD \frac{C_{\rm s} - C_{\rm b}}{\delta},\tag{6}$$

where D is the effective diffusion coefficient that takes into account the contributions from transport by migration [47], $C_{\rm s}$ is the surface concentration, $C_{\rm b}$ is the bulk concentration, and δ is the diffusion layer thickness.

The Nernst diffusion layer concept has frequently been used to obtain a simplified description of mass transport effects in the high-rate anodic dissolution of metals [9, 10, 47, 49]. A stagnant diffusion layer of thickness δ is thus assumed to exist at the anode. Inside the diffusion layer, a concentration gradient exists, and the transport occurs

exclusively by diffusion. Outside the diffusion layer, transport occurs by convection, and the electrolyte concentration is assumed to be constant. The thickness of the anodic diffusion layer depends on hydrodynamic conditions and is given by

$$\delta = \frac{L}{Sh},\tag{7}$$

where L is a characteristic length and Sh is the Sherwood number that represents nondimensional mass transport rate. The Sherwood number can also be regarded as the normalized or nondimensionalized diffusion layer thickness. An exhaustive list of derived expressions describing Sh = f(Re, Sc) are available in the literature for various flow situations and geometries [64]. For a rotating disk electrode,

$$Sh = 0.62 Re^{1/2} Sc^{1/3}, (8)$$

while for a flow channel cell under laminar conditions [9],

$$Sh = 1.85 \left(ReSc \frac{D_h}{L} \right)^{1/3}; \tag{9a}$$

under turbulent conditions [9],

$$Sh = 0.22 Re^{7/8} Sc^{1/4}, (9b)$$

where $Re \ (= D_h v/\nu)$ is the Reynolds number that characterizes the flow, and $Sc \ (= \nu/D)$ is the Schmidt number; D_h is the hydraulic diameter, v is the flow velocity, and v is the kinematic viscosity.

An increase in current density leads to an increase in the rate of metal ion production at the anode. When the metal ion concentration at the surface exceeds the saturation limit, precipitation of a thin salt film occurs. The polarization curve under these conditions exhibits a limiting current plateau. At the limiting current, i_1 , Equation (6) becomes

$$i_{\rm l} = nFD \, \frac{C_{\rm sat}}{\delta},\tag{10}$$

where $C_{\rm sat}$ is the saturation concentration of the precipitating salt at the surface. The electrolyte is assumed to contain a negligibly small concentration of metal; hence, $C_{\rm b}$ is taken to be zero.

The influence of hydrodynamic conditions and electrolyte composition on the limiting current has been investigated in many ECM and electropolishing systems [9–14, 47, 49]. A typical plot showing i_1 as a function of δ for iron and nickel dissolution in a chloride electrolyte is shown in **Figure 8** [9]. Similar results have been obtained in chlorate and nitrate electrolytes [10]. A straight line with a slope of -1 was observed, indicating a mass-transport-controlled process. Similar results have also been reported for many electropolishing systems [12, 39, 42, 65].

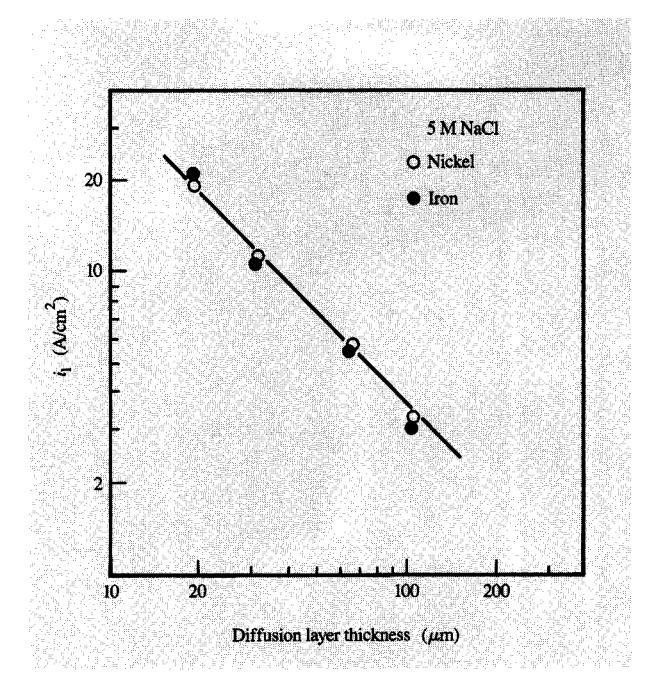


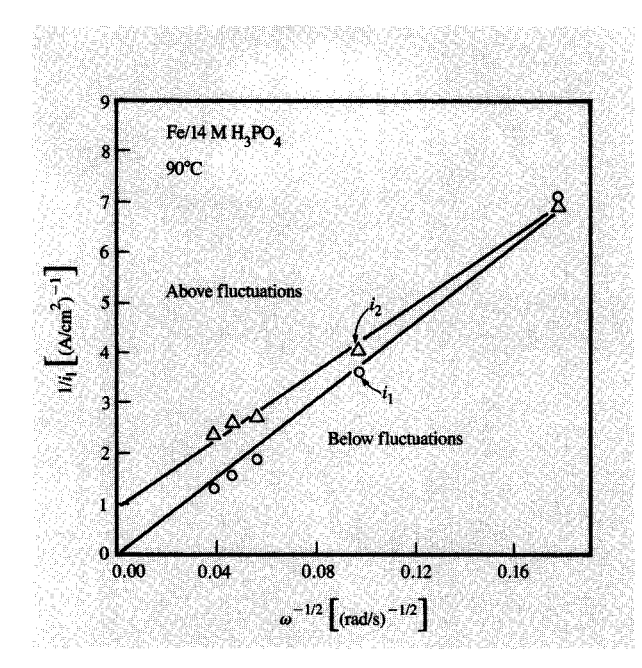
Figure 8

Limiting current densities for iron and nickel dissolution in 5 M NaCl as a function of diffusion layer thickness in a flow channel cell at different flow velocities. From [9], reproduced with permission from Pergamon Press.

In some cases, the influence of convective mass transport may be masked by the presence of a kinetic step (charge transfer, chemical reaction). For a first-order reaction proceeding under mixed (kinetic as well as mass transport) control, the limiting current density measured by a rotating disk electrode can be expressed as

$$\frac{1}{i_1} = \frac{1}{i_k} + \frac{1}{B\omega^{1/2}},\tag{11}$$

where i_k is the kinetic current density that depends on the charge transfer or chemical reaction and is independent of the rotation speed, B is a constant, which for a rotating disk electrode is equal to $0.62nFD^{2/3}\nu^{-1/6}\Delta C$. Equation (11) allows one to evaluate the relative importance of kinetic and mass-transport-controlled steps in the anodic dissolution process. In Figure 9, the inverse of the limiting currents for anodic dissolution of iron in 14 M phosphoric acid at potentials below and above fluctuations [from Figure 2(a)] are plotted as a function of $\omega^{-1/2}$. It is interesting to note that below the current fluctuations, the plot of $1/i_1$ vs. $\omega^{-1/2}$ passes through the origin in accordance with Levich behavior, indicating that the anodic reaction below the fluctuations is mass-transport-controlled. On the other hand, the i_1 values above the



Plots of the inverse of limiting currents below and above current fluctuations for iron in phosphoric acid [Figure 2(a)] as a function of $\omega^{-1/2}$.

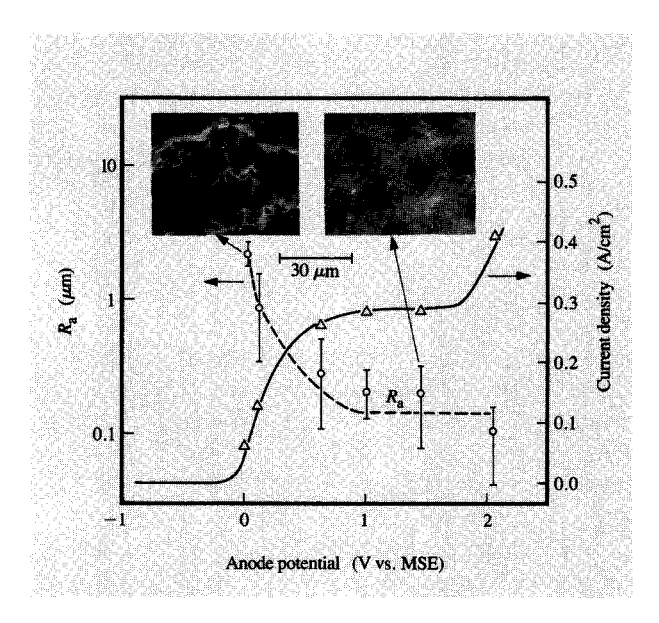


Figure 10

Average surface roughness $R_{\rm a}$ of iron anodes dissolved at different potentials in a mixture of phosphoric-sulfuric acids (2:1) at 90°C [42]. Scanning electron micrographs of anode surfaces at two different potentials are also shown.

current fluctuations show an intercept, indicating the presence of a kinetic step during the dissolution reaction.

A quantitative evaluation of the mass transport processes during nickel dissolution in a nitrate solution has been performed by using different concentrations of nickel nitrate in the electrolyte [47]. The results indicated that the limiting current is observed when the saturation concentration of nickel nitrate is reached at the anode surface, leading to precipitation of a salt film. Salt precipitation has been found in several other ECM systems [9, 10, 13, 14, 49]. Recent studies involving electropolishing of iron and iron-based alloys have also conclusively demonstrated the involvement of the mass transport of reaction products and salt film precipitation at the surface [12, 39, 42].

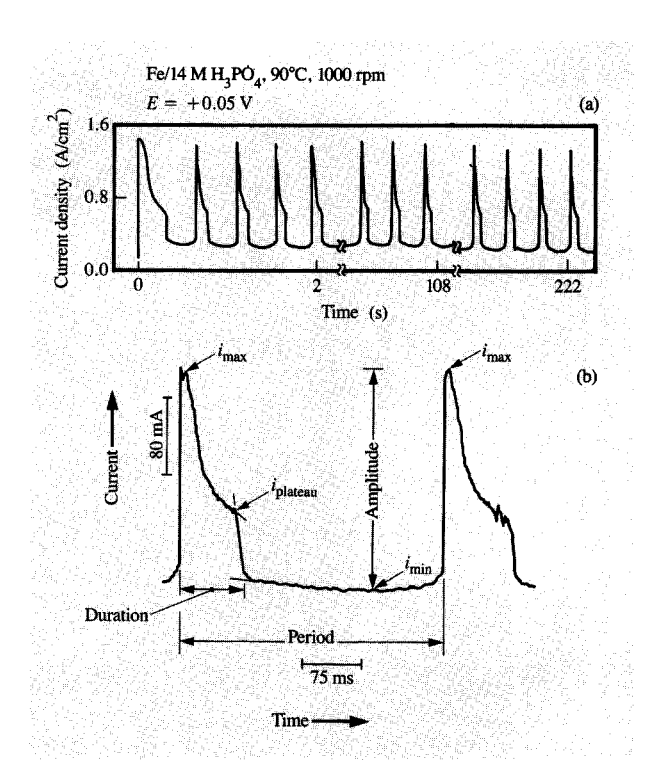
The formation of salt films on the anode influences the surface morphology and the rate of dissolution during ECM and electropolishing [9-14, 39, 42, 47, 49, 66]. Different studies have conclusively demonstrated that two distinctly different surface morphologies result from dissolution. At low current densities, surface etching is observed which, depending on the metal-electrolyte combination, reveals crystallographic steps and etch pits, preferred grain boundary attack, or finely dispersed microstructure. Anodic dissolution under these conditions leads to extremely rough surfaces, as shown in Figure 10. On the other hand, the formation of salt films at the surface suppresses the influence of crystallographic orientation and surface defects on the dissolution process, leading to microfinishing. The presence of salt films may increase the anode potential to such high values that dissolution reactions involving a higher oxidation state or the onset of oxygen evolution may become possible [9, 12, 14, 39, 42].

The presence of salt films has been found to have a significant effect on the current distribution during EMM of photoresist-masked anodes [55]. Below the limiting current, widely spaced patterns were found to dissolve more rapidly than closely spaced patterns because the current distribution under those conditions was primarily dependent on the electrical field in the interelectrode gap. In the presence of salt films, the nonuniformity of the electrical field plays a minor role, the rate of dissolution being governed by local hydrodynamic conditions. Therefore, at the limiting current, at which the current distribution depends on the rate of transport of dissolution products from the anode into the bulk, uniform dissolution occurs independently of pattern spacing [55]. The important role of surface layers of dissolution products in influencing the shape profiles during EMM has been emphasized in several publications [67, 68].

Very little information is available on the thickness and electrical properties of the salt films that form under high-rate dissolution conditions. Ellipsometry [69] and impedance [70] data have indicated that the thickness of the surface film during the electropolishing of copper in phosphoric acid is in the range of 40-120 Å. Kojima and Tobias [65] have reviewed the published impedance data for copper dissolution in phosphoric acid obtained at high frequency, and have interpreted the data by postulating the presence of a thin oxide layer (10-100 Å) through which the transport of copper ions takes place under high-field conduction. For the same system, Glarum and Marshall [70] have obtained low-frequency impedance spectra having a negative real part associated with an inductive behavior. They have attributed the behavior to a decrease in the charge due to the modulation of the flow of ions into the diffusion layer. The capacity associated with the highfrequency loop at high potentials could be represented by a Mott-Schottky plot indicating the presence of a surface layer of uniform charge [70]. Clerc and Landolt [71] have employed ac impedance measurements to investigate the anodic films on nickel at the limiting current in a concentrated lithium chloride solution. They interpreted their experimentally obtained impedance spectra in terms of an equivalent circuit derived from a physical model in which the electrode was assumed to be covered with a thin barrier film through which metal ions are transported under high field conduction. The barrier film was assumed to be covered by an outer porous salt film. The thickness of the barrier layer was estimated to be of the order of 10 nm, and the outer salt film behaved like an ohmic resistor. A similar duplex model for the salt film has also been suggested for copper dissolution in sulfuric acid [72, 73] and for iron dissolution in concentrated phosphoric acid [39].

Periodic phenomena

Periodic fluctuations of current or potential are encountered in many ECM and electropolishing systems [10, 14, 39, 42, 59, 70, 74]. The majority of the reported fluctuations have involved active-passive or passive-transpassive transitions during the anodic polarization of metals. The large body of literature available on this subject has been reviewed by several authors, and several schemes have been proposed for the periodic growth and breakdown of the electrode resistance [74-77]. For dissolution of iron in sulfuric acid, Frank has developed a general theory in which local changes in pH are responsible for the periodic current fluctuations [75]. The changes in solution pH brought about by electrode reactions coupled with diffusion may shift the Flade potential for active-passive transitions. The sequential formation, oxidation, and chemical dissolution of a salt or an oxide layer may induce the transitions [74]. The depletion and accumulation of an acceptor anion necessary for active dissolution may also lead to such fluctuations [74]. Dielectric or mechanical disruption of the resistive



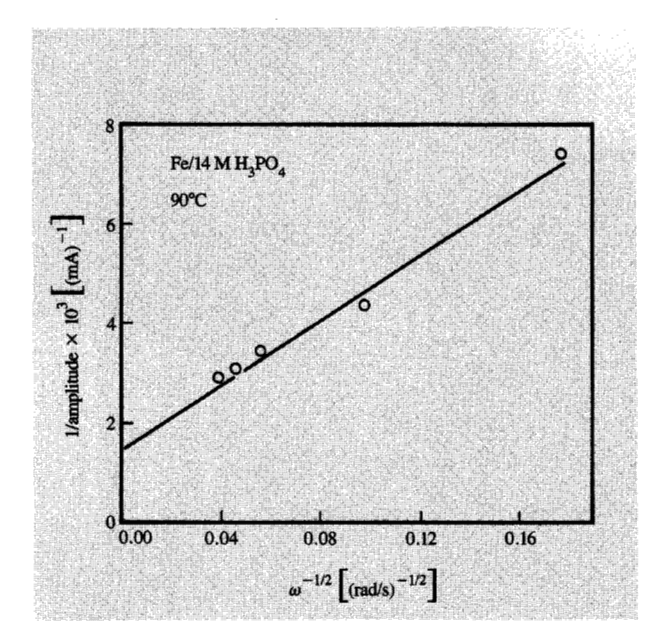
igure 11

(a) Periodic current fluctuations during anodic polarization of iron in 14 M $\rm H_3PO_4$ at a potential of 0.05 V; electrolyte temperature: 90°C, RDE rotation speed: 1000 rpm. (b) Expanded view, depicting fluctuation amplitude and period [39].

layer may alternate with periods of film growth and repair [77]. The periodic current fluctuations may arise from changes in the stoichiometry of anodically formed solid layers [76].

The periodic current fluctuations observed during the anodic polarization of iron in phosphoric acid [Figure 2(a)] have been analyzed further. Part (a) of Figure 11 shows a set of current fluctuations observed at various intervals during potentiostatic anodic polarization at 0.05 V. After an initiation time, the general characteristics of the individual fluctuating pulses are reproducible over an extended period of time. An expanded view of the current fluctuations observed is shown in part (b) of the figure. After an abrupt jump to a peak value, i_{max} , the current slowly decays and reaches a plateau value, i_{plateau} , then drops to a minimum value, i_{\min} . The influence of the applied potential, disk rotation speed, and temperature on the periodic characteristics has been investigated [39]. The potential range of current fluctuations under these conditions is from -0.1 to +0.15 V. The dissolution valence in this potential range is 2.5, which corresponds to the simultaneous formation of Fe²⁺ and Fe³⁺.





Inverse of oscillation amplitude as a function of $\omega^{-1/2}$ [39]. The straight line and nonzero intercept are indicative of mixed (mass transport and kinetic) control of the anodic polarization reactions.

The amplitude of the current fluctuations has been found to increase with increasing rotation speed, indicating that mass transport effects play an important role. In Figure 12, the inverse of the amplitude has been plotted versus the inverse of the square root of the disk rotation speed, in accordance with Equation (11). The straight line and positive intercept indicate the mixed control nature of the reaction, as previously observed for the current plateau i_2 above the fluctuations (Figure 9). The current fluctuations were observed in a potential range situated between two limiting current plateaus, one corresponding to the formation of a salt layer at the surface that is masstransport-controlled, the other corresponding to a mixed control. Periodic fluctuations in this system may therefore represent instabilities associated with the switching between these two film formation processes in the intermediate potential range.

The oscillation period was found to increase with an increase in potential but remained independent of dissolution time. The amplitude of the fluctuations also showed a similar dependence. The dependencies imply that the charge associated with the fluctuations is an increasing function of potential. The charge per oscillating pulse was calculated by integrating the area under each trace of current vs. time. Indeed, the charge was found to increase with increasing potential, indicating that the film thickness increased with potential [78]. The electrolyte temperature

had an insignificant influence on the fluctuation characteristics.

The above results suggest that the periodic oscillations observed during the electropolishing of iron in phosphoric acid are associated with cyclic growth and removal of surface films, accompanied by periodicity in the anodic reaction stoichiometry that switches between the formation of Fe²⁺ and Fe³⁺.

Periodic fluctuations have been observed in many ECM systems, including Cu/sodium chlorate and Fe/sodium chlorate systems. An extensive study of the periodic phenomena observed in a Cu/sodium chlorate system has been conducted by Cooper et al. [74], who interpreted the periodic oscillations as sequential periods of film growth, field collapse, and partial dissolution and removal of film material. Field collapse was considered to follow the onset of resistive switching transitions, while film dissolution/removal took place at discrete sites on the anode. The periodic fluctuations observed in the Fe/sodium chlorate system may be related to the production of chloride ions by chlorate reduction at the anode [10]. However, the effects of the electrolyte anions on the properties of growing surface layers are not yet clear.

Pulsed dissolution

Electroplating by means of a pulsating current and its advantages have been well documented in the literature [79]. Recent studies have shown that a pulsating current can also be advantageously employed in electrochemical machining and finishing [5, 80, 81]. An important aspect of the use of a pulsating current is the possibility of varying mass transport conditions at the anode by independently varying pulse parameters [82]. In the following, a short discussion of mass transport during pulsed anodic dissolution is presented. In principle, either current or voltage pulses of any shape can be applied. The discussion is restricted to rectangular current pulses separated by zero currents.

For a pulsating current, the average current density i_{\bullet} is

$$i_{\rm a} = i_{\rm p} \frac{t_{\rm p}}{t_{\rm p} + t_{\rm p}'} = i_{\rm p} \gamma,$$
 (12)

where i_p is the peak current density, t_p is the pulse on time, and t_p' is the pulse off time. The ratio $t_p/(t_p + t_p')$ is defined as the duty cycle γ .

Mass transport in pulse electrolysis is a combination of steady-state and nonsteady-state diffusion processes. In pulsed ECM (PECM), mass transport has been characterized by a duplex diffusion layer model [82], similar to that proposed by Ibl [83] for pulse plating. According to the model, a stagnant diffusion layer of thickness δ exists at the dissolving anode, the value of δ depending on the hydrodynamic conditions that apply. The presence of a pulsating current leads to the formation of a

time-dependent diffusion layer of thickness δ_p close to the anode surface within which the dissolved metal ion concentration is a periodic function of time. The diffusion layer thickness δ_p is predicted to be

$$\delta_{p} = \left[\frac{4}{\pi} Dt_{p} (1 - \gamma)\right]^{0.5}.$$
(13)

The pulse-limiting current density is defined as the peak current density at which the surface concentration reaches $C_{\rm sat}$ at the end of the pulse. Its predicted behavior is given by the expression [81]

$$i_{\rm pl} = i_{\rm l} \left[\frac{\delta_{\rm p}}{\delta} (1 - \gamma) + \gamma \right]^{-1}. \tag{14}$$

Thus, by suitable choice of the magnitude of the pulse parameters, it should be possible to achieve high instantaneous mass transport rates even at low electrolyte flow rates. An analysis aimed at predicting electrolyte heating in narrow gaps under pulsed ECM conditions has indicated that the instantaneous and average electrolyte heating can be minimized by working with a small "pulseon" time and a low duty cycle [82]. On the other hand, one of the serious drawbacks of pulsed dissolution is that the average current, and hence the average metal removal rate, is very low. Experimental results obtained under well-controlled hydrodynamic conditions in a flow channel cell using passivating and nonpassivating systems have indicated that a good surface finish and high current efficiency for metal dissolution can be obtained even at low average current densities [84]. Figure 13 compares the current efficiency for nickel dissolution in a nitrate electrolyte as a function of current density, obtained by direct current and pulsed current dissolution [84]. It is interesting to note that at a current density at which most of the current is consumed for O2 evolution in dc operation, the use of a pulsed current yields nearly 100% metal dissolution. This behavior permits the dissolution of passivating metals under transpassive conditions with a high current efficiency without the need for a high average current density and high electrolyte flow.

The above concepts have been used to develop an electrochemical saw for maskless metal cutting [80]. Recently, pulsed EMM has been used to fabricate an array of high-precision, microsmooth nozzles in metal foils, for use in ink-jet printers [5]. Pulsed dissolution has been found to be particularly suitable for the through-mask micromachining of thin films, an application in which low dissolution rates are desirable in order to achieve control over the machining process [5].

Alloy dissolution

A heterogeneous alloy can be regarded as a galvanic couple in which electrical connection is achieved by direct

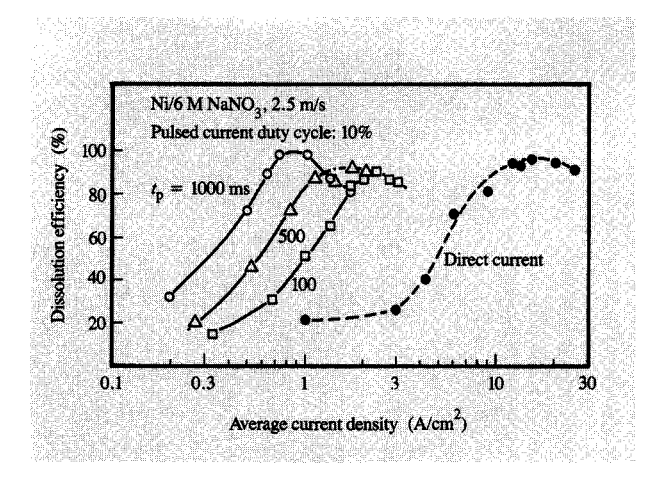


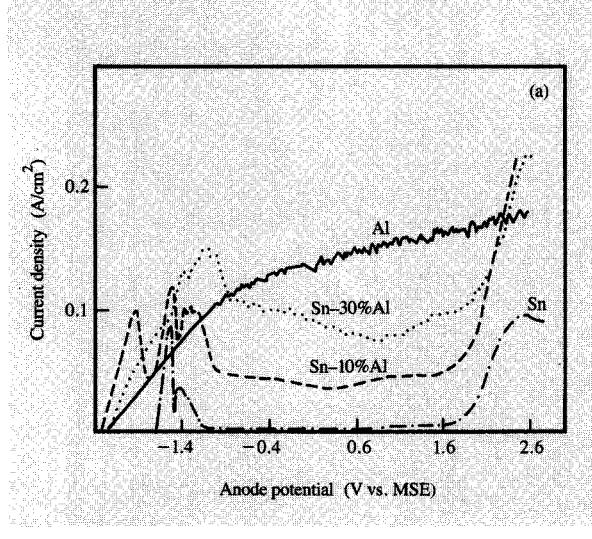
Figure 13

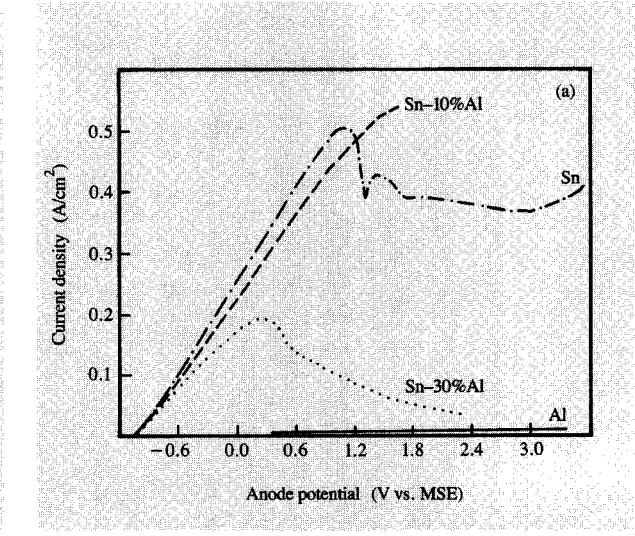
Current efficiency for nickel dissolution in 6 M NaNO₃ as a function of average current density. From [84], reproduced with permission from Pergamon Press.

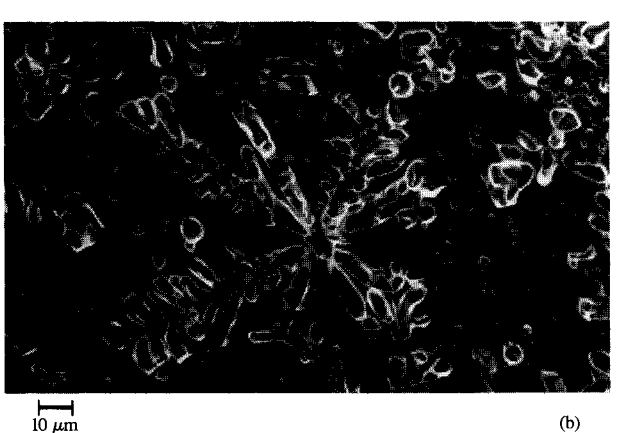
contact. Each phase in a heterogeneous alloy has a certain characteristic polarization behavior which remains unaffected by the fact that it is in an alloy. High-rate anodic dissolution of such alloys may lead to selective dissolution of one of its components, yielding an extremely rough surface. ECM and electropolishing processes are seldom used for their machining. On the other hand, selective dissolution by potentiostatic polarization can be effectively employed to remove an active layer which is in contact with relatively passivating metal layers [85]. By comparing the anodic polarization curves in an appropriate electrolyte, it is possible to select a potential at which a particular layer or a phase is preferentially dissolved. This technique has been employed in the investigation of the three-dimensional morphology of dendrites on Sn-Al alloy specimens by selective dissolution [86]. In this alloy, Al dendrites grow in a Sn matrix. In strong alkaline solutions, the Al dendrites can be selectively dissolved by potentiostatic polarization of the Sn-Al at a potential at which the Sn remains passive (Figure 14). In an acidic potassium sulfate solution, the Al is protected by the formation of an oxide film while the interdendritic matrix (Sn) dissolves, thereby revealing the dendrites (Figure 15).

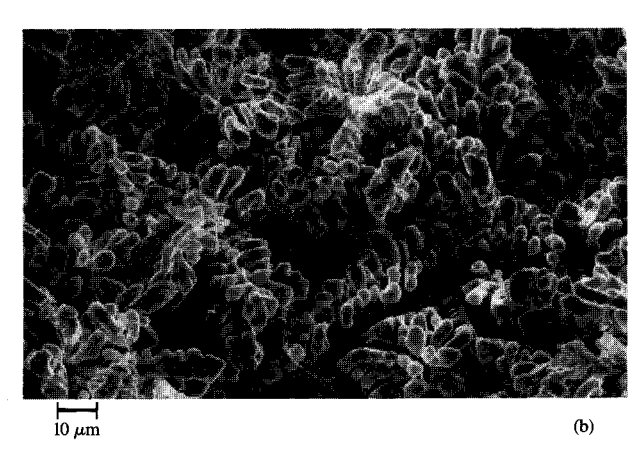
The steady-state dissolution behavior of a single-phase alloy may involve the simultaneous or selective dissolution of its components. In simultaneous dissolution, the alloy constituents go into the solution in stoichiometric proportion; in selective dissolution, the less noble constituent dissolves preferentially, leaving behind a porous metal phase enriched in the more noble component.

In the corrosion literature, the best-known selective dissolution phenomenon is the dealloying of brass, leading









(a) Potentiodynamic anodic polarization curves for Al, Sn, Sn-10%Al, and Sn-30%Al in 1 M NaOH; scan rate: 20 mV/s. (b) Scanning electron micrograph of a Sn-10%Al sample dissolved at $-0.4~\rm V$ vs. MSE for five minutes, showing selective dissolution of Al dendrites. From [86], reproduced with permission from Praktische Metallographie.

Figure 15

(a) Potentiodynamic anodic polarization curves for Al, Sn, Sn-10%Al, and Sn-30%Al in 0.5 M $\rm K_2SO_4$; pH = 1, scan rate: 20 mV/s. (b) Scanning electron micrograph of a Sn-10%Al sample dissolved at -0.5 V vs. MSE for ten minutes, showing selective dissolution of interdendritic Sn matrix. From [86], reproduced with permission from *Praktische Metallographie*.

to dezincification [87]. Some of the other alloy systems that exhibit selective dissolution are Cu-Ni, Cu-Cd, Cu-Au, Ag-Au, and Ag-Pd [88-93]. During the selective dissolution of Ag-Au and Cu-Ag alloys, overvoltage has been found to increase with increasing gold content [90]. Above a critical gold concentration, the polarization behavior coincides with that for oxygen evolution on pure gold [90]. The formation of a porous metal phase resulting from the selective dissolution has been confirmed by several studies. For example, X-ray diffraction studies of selectively dissolved Cu-Au alloys have indicated that the

porous layer represents a new phase enriched in gold [94]; double-layer capacity measurements have confirmed that the formation of the porous layer coincides with a large increase in the anode surface area [91]. During the selective dissolution of Cu–Pd and Ag–Pd, AES analysis has indicated surface enrichment of Pd, the surface concentration being dependent on the bulk concentration and dissolution potential [92, 93]. Several mechanisms have been proposed to explain the selective dissolution of single-phase alloys and formation of the porous layer. According to Tischer and Gerischer [90], the selective

dissolution is governed by the surface mobility of the noble component. Pickering and Wagner [94] have proposed that solid-state diffusion of the noble component occurs from the bulk to the surface because of the presence of divacancies.

Most of the alloys that are important in ECM and electropolishing exhibit simultaneous dissolution. Steigerwald and Green have proposed an empirical procedure for the prediction of the anodic polarization curve of a simultaneously dissolving alloy from that of its components [95]. Bockris et al. [96] have studied the dissolution of CuNi alloys and have evaluated an apparent exchange current density for the different alloys they examined. The rate constant for dissolution was found to vary with alloy composition. No surface enrichment of Pd was observed during the simultaneous dissolution of Ag-Pd alloys with Pd concentration greater than 50% [93]. The anodic polarization behavior of Fe-Cr alloys has been studied in sodium chloride and sodium nitrate solutions [55, 81]. Figure 16 shows the anodic polarization behavior observed for Fe, Cr, and their alloys in 5 M NaCl. It is interesting to note that the polarization behavior of Fe24Cr is similar to that of pure Cr, while the polarization behavior of Fe13Cr is close to that of pure Fe. Both Fe and Fe13Cr exhibit a current plateau because of the formation of a salt film [55]. Cr and Fe24Cr dissolve at transpassive potentials and do not exhibit a current plateau. The anodic behavior of 304 stainless steel (Fe10Ni18Cr) resembles that of Fe13Cr, but a higher current plateau is exhibited. The dissolution valence was determined from weight loss measurements using Equation (3). The atomic weight of the alloy was calculated from

$$M_{\text{alloy}} = \sum x_i M_i, \qquad (15)$$

where x_j is the mole fraction of component j and M_j is its atomic weight. **Table 2** summarizes the available literature data on experimentally determined dissolution stoichiometry for some selected iron-based alloys. In

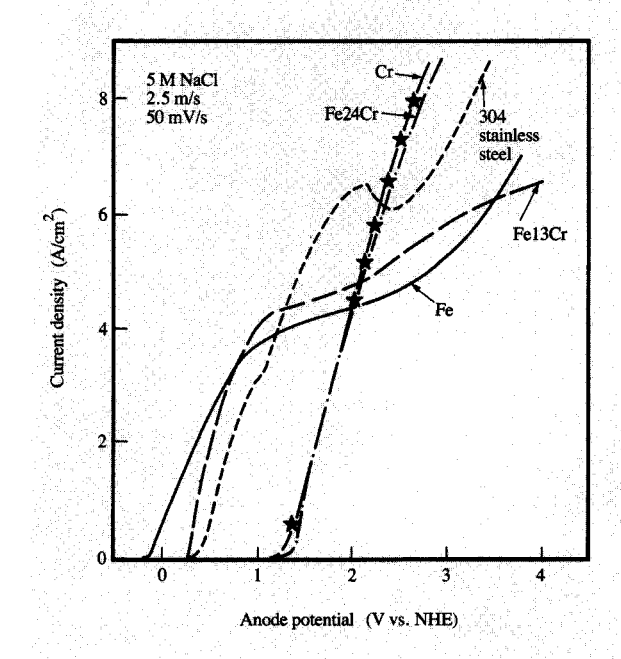


Figure 16

Potentiodynamic anodic polarization curves for Fe, Cr, and their alloys in 5 M NaCl. Experiments were performed in a flow channel cell at a flow velocity of 2.5 m/s and a scan rate of 50 mV/s. From [55], reproduced with permission from Chapman and Hall.

chloride solutions, the dissolution valence for Fe13Cr has been found to be close to 2.1 below the limiting current, indicating that Cr dissolves as Cr^{3+} and iron dissolves as Fe^{2+} , as described earlier. Above the limiting current, a value of n=2.7 has been obtained. This corresponds to Fe dissolution simultaneously forming Fe^{2+} and Fe^{3+} , as was obtained for pure Fe and Cr dissolving as Cr^{6+} .

Table 2 Anodic dissolution species for selected iron-based alloys.

Alloy	Electrolyte	Dissolution species		Oxygen evolution	Reference
		Active	Transpassive		
Fe13Cr			Fe ³⁺ , Cr ⁶⁺	yes	11, 12
Fe24Cr	$H_3PO_4 + H_3SO_4$		Fe ³⁺ , Cr ⁶⁺ Fe ³⁺ , Ni ²⁺ , Cr ⁶⁺	yes	12
Fe10Ni18Cr	J 7 2 7	_	Fe ³⁺ , Ni ²⁺ , Cr ⁶⁺	yes	12
Fe13Cr		Fe ²⁺ , Cr ³⁺	Fe ²⁺ , Fe ³⁺ , Cr ⁶⁺ Fe ³⁺ , Cr ⁶⁺ Fe ³⁺ , Ni ²⁺ , Cr ⁶⁺	no	55, 81
Fe24Cr	NaCl	-	Fe^{3+}, Cr^{6+}	no	55, 81
Fe10Ni18Cr		_	Fe ³⁺ , Ni ²⁺ , Cr ⁶⁺	no	55
Fe10Ni18Cr	NaNO,	_	Fe ³⁺ , Ni ²⁺ , Cr ⁶⁺	yes	55
	,			(only in dilute solution)	

Fe24Cr yields a value of n = 3.6, independently of current density level. This corresponds to the formation of Fe³⁺ and Cr⁶⁺. For 304 stainless steel, a value of n = 3.5 at all current densities corresponds to the formation of Fe³⁺, Cr⁶⁺, and Ni²⁺.

The anodic dissolution of different types of iron-based alloys in concentrated acids has been investigated in order to develop understanding of the electropolishing behavior of these alloys [11, 12]. The anodic polarization of Fe13Cr, Fe24Cr, and 304 stainless steel in concentrated phosphoric, sulfuric, and their mixtures has been found to exhibit a typical active-passive-transpassive behavior [11, 12]. In the transpassive potential region, a mass-transportcontrolled limiting current plateau has been observed. At the limiting current, metal components dissolve to form Fe³⁺, Cr⁶⁺, and Ni²⁺. Above the limiting current, oxygen evolution occurs, leading to higher values of the dissolution valence than that predicted by Equations (3) and (15), using the highest oxidation state of the separate components. The measured limiting current has been found to be influenced by the electrolyte temperature and the electrode rotation speed, indicating that the electropolishing of these alloys is controlled by convective mass transport. At low temperatures, the mass transport effects are masked by the presence of kinetic steps. High temperatures, on the other hand, favor the establishment of mass-transport-controlled conditions and lead to the achievement of highly reflecting mirror-finish surfaces. The investigations have indicated that the anodic dissolution and electropolishing behaviors of these alloys are very similar to those of their constituent metals, as described earlier.

Concluding remarks

The literature dealing with high-rate anodic dissolution of metals that is applicable to electrochemical machining and electropolishing has been reviewed. Electrochemical and hydrodynamic parameters influence the nature of anodic reactions and their rates, which in turn influence the performance of metal shaping and finishing operations. Metal removal rate is influenced by parameters which influence anodic reaction stoichiometry. These include the anode potential, the nature and concentration of the electrolyte anions, and the mass transport parameters. Surface finish during high-rate anodic dissolution depends on the mass transport conditions at the anode. At potentials below the limiting current range, rough surfaces are obtained as a result of localized, metallurgically dependent dissolution processes such as crystallographic etching and grain boundary attack. The limiting current, which appears at higher potentials, is mass-transportcontrolled, corresponding to the formation of a salt layer at the anode that suppresses the influence of the metallurgical phenomena on the dissolution process. Dissolution at or

above the limiting current, therefore, yields microsmooth surfaces. The presence of a salt film also influences the current distribution, hence the uniformity of metal dissolution and the shape profiles during through-mask electrochemical micromachining. High-rate anodic dissolution of most of the single-phase alloys that are of interest in electrochemical machining and electropolishing involves dissolution of the alloy constituents in their stoichiometric proportions. The anodic dissolution behavior of these alloys shows similarities to that of their constituent metals. In the application of high-rate dissolution processes to microfabrication, the use of a pulsating current is expected to offer several advantages. The relatively high instantaneous current densities that can be applied with a pulsating current permit the dissolution of metals and alloys with a high efficiency, even at low average currents. Pulsed dissolution is, therefore, considered most suitable for electrochemical micromachining of thin films and foils, where low dissolution rates are desirable for better control over the machining process [5].

References

- J. A. McGeough, Advanced Methods of Machining, Chapman and Hall, New York, 1988.
- 2. W. J. McTegart, The Electrolytic and Chemical Polishing of Metals, Pergamon Press, London, 1956.
- M. Datta and L. T. Romankiw, J. Electrochem. Soc. 136, 285C (1989).
- M. Datta, L. T. Romankiw, D. R. Vigliotti, and R. J. von Gutfeld, J. Electrochem. Soc. 136, 2251 (1989).
- M. Datta, in *Electrochemical Microfabrication*, M. Datta, K. Sheppard, and D. Snyder, Eds., The Electrochemical Society, Inc., Pennington, NJ, 1992, p. 61.
- 6. T. P. Hoar, Corros. Sci. 7, 341 (1967).
- M. Datta and D. Landolt, Oberflache-Surface 19, 159 (1978).
- 8. D. Landolt, in *Passivity of Metals*, R. Frankenthal and J. Kruger, Eds., The Electrochemical Society, Inc., Pennington, NJ, 1978, p. 488.
- 9. M. Datta and D. Landolt, Electrochim. Acta 25, 1255 (1980)
- 10. M. Datta and D. Landolt, *Electrochim. Acta* 25, 1263 (1980).
- L. Ponto, M. Datta, and D. Landolt, Surf. & Coatings Tech. 30, 265 (1987).
- 12. M. Datta and D. Vercruysse, *J. Electrochem. Soc.* 137, 3016 (1990).
- 13. D. Landolf, R. H. Muller, and C. W. Tobias, J. *Electrochem. Soc.* **116**, 1384 (1969).
- 14. K. Kinoshita, D. Landolt, R. H. Muller, and C. W. Tobias, J. Electrochem. Soc. 117, 1246 (1970).
- W. Allgaier and K. E. Heusler, J. Appl. Electrochem. 9, 155 (1979).
- W. J. Lorenz and K. E. Heusler, in Corrosion Mechanisms, F. Mansfeld, Ed., Marcel Dekker, Inc., New York, 1987, pp. 1-83.
- 17. M. Datta and D. Landolt, Corros. Sci. 13, 187 (1973).
- A. Bengali and K. Nobe, J. Electrochem. Soc. 126, 1118 (1979).
- 19. H. C. Kuo and K. Nobe, *J. Electrochem. Soc.* **125**, 853 (1978).
- S. Asakura and K. Nobe, J. Electrochem. Soc. 118, 19 (1971).

- L. Young, Anodic Oxide Films, Academic Press, Inc., New York, 1961.
- J. L. Weininger and M. W. Breiter, J. Electrochem. Soc. 110, 484 (1963).
- 23. D. E. Davies and W. Barker, Corrosion 20, 47t (1964).
- M. Pourbaix, Atlas of Electrochemical Equilibria in Aqueous Solutions, Pergamon-CEBELCOR, Brussels, 1966
- 25. S. U. Falk, J. Electrochem. Soc. 107, 661 (1960).
- A. J. Salkind and P. F. Bruins, J. Electrochem. Soc. 109, 356 (1962).
- T. Dickinson, A. F. Povey, and P. M. A. Sherwood, *JCS Faraday Trans. I* 73, 327 (1977).
- G. W. D. Briggs and W. F. K. Wynne Jones, *Electrochim. Acta* 7, 241 (1962).
- M. Datta, H. J. Mathieu, and D. Landolt, *Electrochim. Acta* 24, 843 (1979).
- M. Cohen, in *Passivity of Metals*, R. P. Frankenthal and J. Kruger, Eds., The Electrochemical Society, Inc., Pennington, NJ, 1978, p. 521.
- M. Nagayama and M. Cohen, J. Electrochem. Soc. 109, 781 (1962).
- M. Nagayama and M. Cohen, J. Electrochem. Soc. 110, 670 (1963).
- C. L. Foley, J. Kruger, and C. J. Bechtoldt, J. Electrochem. Soc. 114, 994 (1967).
- 34. K. J. Vetter, J. Electrochem. Soc. 110, 597 (1963).
- M. C. Bloom and M. Goldenberg, Corros. Sci. 5, 623 (1965).
- N. Sato, K. Kudo, and T. Noda, Corros. Sci. 10, 785 (1970).
- Z. Szklarska-Smialowska, Pitting Corrosion of Metals, National Association of Corrosion Engineers, Houston, 1986.
- W. J. Plieth and K. J. Vetter, Ber. Bunsenges. 74, 1077 (1969).
- L. F. Vega and M. Datta, Electrochemical Society Extended Abstract No. 367, Fall Meeting, Seattle, 1990, p. 531 (extended version to be published).
- T. P. Hoar, D. C. Mears, and G. P. Rothwell, *Corros. Sci.* 5, 279 (1965).
- 41. D. Landolt, Electrochim. Acta 32, 1 (1987).
- 42. M. Datta, L. F. Vega, L. T. Romankiw, and P. Duby, Electrochim. Acta 37, 2469 (1992).
- 43. K. W. Mao, J. Electrochem. Soc. 118, 1870 (1971).
- 44. D. T. Chin, J. Electrochem. Soc. 118, 174 (1971).
- M. A. LaBoda, A. J. Chartrand, J. P. Hoare, C. R. Wiese, and K. W. Mao, J. Electrochem. Soc. 120, 643 (1973).
- K. W. Mao and D. T. Chin, J. Electrochem. Soc. 121, 191 (1974).
- M. Datta and D. Landolt, J. Electrochem. Soc. 122, 1466 (1975).
- 48. J. P. Hoare and C. R. Wiese, *Corros. Sci.* **15**, 435 (1975).
- 49. M. Datta and D. Landolt, *J. Appl. Electrochem.* 7, 247 (1977).
- M. Datta and D. Landolt, J. Electrochem. Soc. 124, 483 (1977).
- 51. D. Landolt, J. Electrochem. Soc. 119, 708 (1972).
- 52. M. Datta and D. Landolt, Proceedings of the 2nd International Symposium on Industrial and Oriented Basic Electrochemistry, SAEST, Madras, India, 1980, p. 4.3.1.
- 53. M. LaBoda and M. L. McMillan, J. Electrochem. Technol. 5, 346 (1967).
- O. A. Arzhintar, A. I. Dikusar, V. I. Petrenko, and Yu. N. Petrov, Electronnaya Orabot. Mat. 6, 9 (1974).
- E. Rosset, M. Datta, and D. Landolt, J. Appl. Electrochem. 20, 69 (1990).
- J. W. Johnson, C. H. Chi, C. K. Chen, and W. J. James, Corrosion 26, 238 (1970).
- 57. M. N. Hull, J. Electroanal. Chem. 38, 143 (1972).

- J. B. Mathieu and D. Landolt, Oberflache-Surface 20, 24 (1979).
- L. Ponto and D. Landolt, J. Appl. Electrochem. 17, 205 (1987).
- K. W. Mao, M. A. LaBoda, and J. P. Hoare, J. Electrochem. Soc. 119, 419 (1972).
- M. Datta, H. J. Mathieu, and D. Landolt, in *Passivity of Metals and Semiconductors*, M. Froment, Ed., Elsevier, Amsterdam, 1983, p. 113.
- M. Datta, H. J. Mathieu, and D. Landolt, Appl. Surf. Sci. 18, 299 (1984).
- M. Datta, H. J. Mathieu, and D. Landolt, J. Electrochem. Soc. 131, 2484 (1984).
- 64. J. R. Selman and C. W. Tobias, Adv. Chem. Eng. 10, 211
- (1978).65. K. Kojima and C. W. Tobias, *J. Electrochem. Soc.* 120, 1026 (1973).
- M. Datta and D. Landolt, J. Electrochem. Soc. 129, 1890 (1982).
- R. C. Alkire and P. B. Reiser, J. Electrochem. Soc. 131, 2795 (1984).
- R. C. Alkire and H. Deligianni, J. Electrochem. Soc. 135, 1093 (1988).
- M. Novak, A. K. N. Reddy, and H. Wroblowa, J. Electrochem. Soc. 117, 733 (1970).
- S. H. Glarum and J. H. Marshall, J. Electrochem. Soc. 132, 2872 (1985).
- 71. C. Clerc and D. Landolt, *Electrochim. Acta* 33, 859 (1988).
- R. C. Alkire and A. Cangellari, J. Electrochem. Soc. 136, 913 (1989).
- 73. C. Clerc and R. C. Alkire, *J. Electrochem. Soc.* **138**, 25 (1991)
- 74. J. F. Cooper, R. H. Muller, and C. W. Tobias, *J. Electrochem. Soc.* 127, 1733 (1980).
- 75. U. F. Frank, Z. Electrochem. 62, 649 (1958).
- K. S. Indira, S. K. Rangarajan, and K. S. G. Doss, J. Electroanal. Chem. 21, 49 (1969).
- J. Wojtowicz, in Modern Aspects of Electrochemistry, Vol. 8, J. O'M. Bockris and B. Conway, Eds., Plenum Press, New York, 1972, Ch. 1.
- H. P. Lee, K. Nobe, and A. J. Pearlstein, J. Electrochem. Soc. 132, 1031 (1985).
- J. C. Puippe and F. Leaman, Theory and Practice of Pulse Plating, American Electroplaters and Surface Finishers Society, Florida, 1986.
- 80. M. Datta and D. Landolt, J. Appl. Electrochem. 13, 795
- E. Rosset, M. Datta, and D. Landolt, *Plat. Surf. Finish.* 71, 60 (1985).
- 82. M. Datta and D. Landolt, *Electrochim. Acta* **26**, 899 (1981).
- 83. N. Ibl, Surf. Tech. 10, 81 (1980).
- M. Datta and D. Landolt, *Electrochim. Acta* 27, 385 (1982).
- M. Datta, S. Krongelb, and L. T. Romankiw, *IBM Tech. Disclosure Bull.* 32, 231 (1990).
- M. Datta, B. Giovanola, and J. Kolub, *Prakt. Met.* 20, 394 (1983).
- U. R. Evans, The Corrosion and Oxidation of Metals, Arnold, London, 1971.
- 88. R. G. Blundy and M. J. Pryor, Corros. Sci. 12, 65 (1972).
- D. S. Kier and M. J. Pryor, J. Electrochem. Soc. 127, 2138 (1980).
- R. P. Tischer and H. Gerischer, Z. Electrochem. 62, 50 (1955).
- 91. H. W. Pickering, J. Electrochem. Soc. 115, 143 (1968).
- J. Gniewek, J. Pezy, B. G. Baker, and J. O'M. Bockris, J. Electrochem. Soc. 125, 17 (1978).
- S. Rambert and D. Landolt, Electrochim. Acta 31, 1421 (1986).

- H. W. Pickering and C. Wagner, *J. Electrochem. Soc.* 114, 698 (1967).
- R. F. Steigerwald and N. D. Green, J. Electrochem. Soc. 109, 1026 (1962).
- J. O'M. Bockris, R. T. Rubin, A. Despic, and B. Lovrecek, Electrochim. Acta 17, 973 (1972).

Received February 7, 1992; accepted for publication November 9, 1992 Madhav Datta IBM Research Division, Thomas J. Watson Research Center, P.O. Box 218, Yorktown Heights, New York 10598 (MADHAV at YKTVMV, madhav@watson.ibm.com). Dr. Datta is a Research Staff Member in the Manufacturing Research Department of the IBM Thomas J. Watson Research Center. He received a B.S. in chemical engineering from the H.B. Technological Institute, Kanpur, India, an M.S. in engineering from the University of California at Los Angeles, and a Ph.D. in electrochemical engineering from the Swiss Federal Institute of Technology (SFIT), Lausanne, Switzerland, in 1975. He worked in the materials department of SFIT until 1984, and in 1984-85, in the Research and Development Center for Iron and Steel, Ranchi, India. In 1985 Dr. Datta joined the Manufacturing Research Department of the Thomas J. Watson Research Center, where his research interests include electrochemical micromachining and polishing. Dr. Datta is an Adjunct Professor of Chemical Engineering at the University of Connecticut at Storrs. He is the North American editor of the journal Processing of Advanced Materials.